

Dynamical Evidence for a Black Hole in GX 339–4

R. I. Hynes^{1,4,7}, D. Steeghs^{2,4}, J. Casares³, P. A. Charles⁴, and K. O’Brien^{5,6}

ABSTRACT

We present outburst spectroscopy of GX 339–4 which may reveal the motion of its elusive companion star. N III lines exhibit sharp emission components moving over $\sim 300 \text{ km s}^{-1}$ in a single night. The most plausible interpretation of these components is that they are formed by irradiation of the companion star and the velocities indicate its orbital motion. We also detect motion of the wings of the He II 4686 Å line and changes in its morphology. No previously proposed period is consistent with periodic behavior of all of these measures. However, consistent and sensible solutions are obtained for periods around 1.7 days. For the best period, 1.7557 days, we estimate a mass function of $5.8 \pm 0.5 M_{\odot}$. Even allowing for aliases, the 95 % confidence lower-limit on the mass function is $2.0 M_{\odot}$. GX 339–4 can therefore be added to the list of dynamical black hole candidates. This is supported by the small motion in the wings of the He II line; if the compact object velocity is not larger than the observed motion then the mass ratio is $q \lesssim 0.08$, similar to other systems harboring black holes. Finally, we note that the sharp components are not always present, but do seem to occur within a repeating phase range. This appears to migrate between our epochs of observation, and may indicate shielding of the companion star by a variable accretion geometry such as a warp.

¹The University of Texas at Austin, Astronomy Department, 1 University Station C1400, Austin, Texas 78712, USA; rih@astro.as.utexas.edu

²Harvard-Smithsonian Center for Astrophysics, 60 Garden Street, MS-67, Cambridge, MA 02138, USA; dsteeeghs@head-cfa.harvard.edu

³Instituto de Astrofísica de Canarias, 38200 La Laguna, Tenerife, Spain; jcv@ll.iac.es

⁴Department of Physics and Astronomy, University of Southampton, Southampton, SO17 1BJ, UK; pac@astro.soton.ac.uk

⁵European Southern Observatory, Casilla 19001, Santiago 19, Chile; kobrien@eso.org

⁶School of Physics and Astronomy, University of St Andrews, St Andrews KY16 9SS, UK

⁷Hubble Fellow

Subject headings: accretion, accretion disks — binaries: close — X-rays: binaries
— stars: individual: V821 Ara

1. Introduction

Most Galactic black holes are found in transient low-mass X-ray binaries (LMXBs), where bright X-ray outbursts are interspersed with long quiescent periods when the optical light is typically dominated by the companion star. Although one of the earliest proposed black hole candidates (Samimi et al. 1979), GX 339–4 remains one of the most inaccessible to direct measurement of system parameters due to a higher level of X-ray activity; even when the X-rays are at their faintest, the companion star remains undetectable (Shahbaz, Fender, & Charles 2001). Several orbital periods have been proposed based on both photometric and spectroscopic observations (0.62 days; Callanan et al. (1992); 0.7 days; Cowley et al. (2002)), but even this most basic of binary parameters remains in dispute. Without detecting the companion star in quiescence, this problem seems insurmountable. However an approach was suggested by the discovery by Steeghs & Casares (2002) of sharp N III emission components in the bright persistent low-mass X-ray binary Sco X-1. They were associated with the irradiated companion star and yielded the first radial velocity curve of the companion, and hence the first credible estimate of the binary parameters.

When GX 339–4 entered a bright X-ray outburst in mid-2002, we sought to apply this method. Initial observations used the NTT and AAT; follow-up VLT observations were also obtained. The average *RXTE*/ASM count rates⁸ corresponded to 0.46 Crab at the first epoch and 0.84 Crab at the second. Here we report the detection of the companion star in the N III lines, a new orbital period estimate, and the derived mass function of the compact object. A future work will perform a thorough analysis of other aspects of this rich dataset.

2. Observations

Medium dispersion spectroscopy was obtained with the ESO NTT on 2002 June 8–11 using EMMI. Details of all our observations are given in Table 1. On June 8 and 10 we operated the red-arm with the MIT/LL detector and grating #6, yielding a wavelength coverage of 4410–5160 Å. In poorer conditions on June 9 we used the blue arm, TK1034, and grating #3 resulting in a lower resolution and wavelength coverage 4500–4960 Å. Data

⁸Based on quick-look results provided by the ASM/RXTE team.

reduction was done in IRAF to remove the bias level, flat-field, and optimally extract the spectra (Horne 1986). Wavelength calibrations used contemporaneous HeAr (red-arm) or ThAr (blue-arm) arc lamp observations. The slit was aligned to also include a nearby K star (star 2 of Grindlay (1979)). This was rich in absorption lines and so allowed a frame-by-frame check of the stability of the wavelength calibration.

We also used the RGO Spectrograph attached to the AAT over 2002 June 6–11, with the R1200B grating yielding a wavelength coverage of 3500–5250 Å. The images were de-biased and flat-fielded, and the spectra subsequently extracted using conventional optimal extraction techniques (Horne 1986). Wavelength calibrations were interpolated between CuAr comparison lamp images, obtained every 20–30 mins.

A final series of spectra was obtained using UVES at the VLT on 2002 August 9–15. Six sets of five spectra were obtained in an identical configuration; the red-arm was used with the EEV+MIT/LL mosaic and cross-disperser #3, yielding a wavelength coverage of 4100–6200 Å. Pipeline optimal extractions were supplied and were of good quality. Some spectra exhibited a narrow dip within the Bowen blend; these appear spurious and were masked out of our fits.

3. Radial velocities and the orbital period

3.1. The sharp Bowen components

The spectrum around 4640 Å is dominated by two or three emission components (e.g. Fig. 1). These are N III 4634 and 4641/42 Å, which are always present and C III 4647/50/51 Å, which is sometimes as strong as the N III lines and sometimes nearly absent. This decomposition is the same as suggested for Her X-1 (Still et al. 1997) and Sco X-1 (Steeeghs & Casares 2002). We will refer to these lines as the Bowen blend, although the C III emission is not formed by Bowen fluorescence. For a radial velocity analysis, we selected only those spectra with sharp components. The resulting dataset comprised all the NTT red-arm spectra and 7 of the VLT spectra. No sharp components were detected in the AAT or NTT blue spectra, neither were they present in the remainder of the VLT spectra. In our ‘sharp component’ spectra, we measure average component FWHM of 270 km s⁻¹ at the June epoch and 350 km s⁻¹ at the second, with no significant width modulation within each epoch.

For each spectrum showing sharp components, we fit with a model comprising two sets of Gaussian lines, corresponding to N III 4634/41/42 Å and C III 4647/50/51 Å. The relative ratios within each species were fixed to the values given by McClintock, Canizares, & Tarter (1975). We allowed the relative strengths of the N III and C III groups to vary, and

fitted for the N III and C III velocities. The C III velocities were discarded as these lines were often barely detectable, and the uncertain ratios of the unresolved 4647/50/51 Å components renders the effective wavelength of the C III blend uncertain. The N III velocities were always well constrained, as the 4634 Å line is well separated from the others. The most dramatic changes were in the NTT red-arm data, for which we obtained a continuous night of data, about 9 hrs. During this period we saw a monotonic trend spanning $\sim 300 \text{ km s}^{-1}$. Such narrow components moving at high radial velocity can only readily be explained as due to the orbital motion of the companion star. The measured components widths are larger than the expected rotational broadening, in particular during our VLT observations. Outflows driven by the X-ray irradiation may be one source of additional broadening mechanisms.

We combined all of the velocities and fitted sinusoidal radial velocity curves as a function of orbital period. We used a grid of trial periods from 0.1–2.5 days, with a separation of 10^{-4} days, enough to resolve individual minima. We plot the minimum χ^2 as a function of period in Fig. 2a. There are clearly many possible solutions, corresponding to periods around 0.7, 0.85, 1.2, or 1.7 days, but the 0.62 day period of Callanan et al. (1992) is ruled out. As we will argue, the preferred period is 1.7557 days, and the N III velocities are folded on this period in Fig. 3a.

3.2. He II wings

To further constrain the orbital period, we applied the double Gaussian method of Schneider & Young (1980) and Shafter (1983) to trace the motion of the He II line wings in the VLT spectra. These may follow the orbit of the compact object, but even if they are contaminated then any motion should still be on the orbital period. We use all of the VLT spectra for this analysis. As for the N III velocities, we fit a sinusoidal radial velocity curve as a function of orbital period and derive the periodogram shown in Fig. 2b. The only periods common to both the N III data and the He II line wings are around 0.7 and 1.7 days. We initially favored the former, as this value had previously been suggested by Cowley et al. (2002). A significant difficulty with this period, however, is that nearly all the N III velocities measured correspond to blue-shifts. For an 0.7 day period, almost the full range of radial velocities should have been sampled and so the systemic velocity of the companion star would have to be extremely large, $\sim -150 \text{ km s}^{-1}$. The systemic velocity inferred from the He II wings, however, is small, only 10 km s^{-1} . This inconsistency led us to consider whether the longer period might actually be the correct one as this results in consistent and small systemic velocities.

3.3. Line morphology changes

An outstanding question is why only some N III profiles show sharp components, all corresponding to blue-shifts. One might naturally expect this to reflect orbital morphology changes, but this is not the case for the 0.7 day period; in this case, spectra showing sharp components overlap in phase with those which do not. On the 1.7 day period, however, the two types of profiles are cleanly segregated and do not overlap; this supports the idea that we are seeing orbital motion of a companion star which is only visible, or only illuminated, at certain orbital phases.

A related problem is that in the long NTT run, the He II line always showed a blue-shifted peak. As for N III, this is hard to explain with an 0.7 day period as other spectra at the same implied orbital phase do not show this asymmetry. We can quantify it by fitting a single broad Gaussian profile to He II, and this line is strong enough that we can use *all* of our first epoch data. The derived radial velocity curve will not have much physical significance, but this does provide a quantitative way to assess which trial periods yield repeatable changes in the line symmetry. The periodogram, derived as above, is shown in Fig. 2c. As for the appearance of sharp Bowen components, the He II symmetry changes are modulated on the 1.7 day period, but not clearly on the 0.7 day one.

3.4. The derived orbital period

We conclude that only a period close to 1.7 days is consistent with the N III velocities and appearance of sharp components; the He II wing velocities; and the changes in the He II morphology. This period has the advantage, unlike the others, that a consistent and sensible (i.e. close to zero) systemic velocity is derived for both N III lines (which we believe trace the companion star velocity) and He II wings. Several aliases (from the most precise Bowen fit) are consistent with the He II data. The best overall fit is for $P_{\text{orb}} = (1.7557 \pm 0.0004)$ days, but 1.7104 ± 0.0006 days or 1.6584 ± 0.0017 days are also possible.

4. The system parameters

Having identified the best-fitting orbital period, we can now fit for orbital velocities. The most straightforward is the N III modulation, which must originate from the companion star. We show the fit to the data in Fig. 3a. The limited phase coverage obviously compromises the accuracy of our results, and we find there is a range of solutions with K_2 and γ positively correlated. For the 1.7557 day period, the best fit is $K_2 = (317 \pm 10) \text{ km s}^{-1}$, where the

error is a 1σ confidence region with γ left unconstrained. This best fit corresponds to $\gamma \sim 30 \text{ km s}^{-1}$, measured with respect to the local standard of rest. For the 1.7104 day period $K_2 = (289 \pm 10) \text{ km s}^{-1}$ and for 1.6584 days, $K_2 = (241 \pm 8) \text{ km s}^{-1}$. A more conservative constraint is to consider all three aliases as equally valid. We then derive a 95% confidence lower limit on K_2 of 226 km s^{-1} , corresponding to the 1.6584 day period. These values are all strictly lower limits for K_2 , as N III lines will be formed on the inner, irradiated face of the companion star. Thus they do not trace the motion of its center of mass, but instead have a somewhat *lower* velocity.

From these combinations of P_{orb} and K_2 , we then derive corresponding mass functions. Our best period corresponds to $f(M) = (5.8 \pm 0.5) M_{\odot}$, whereas the 95% lower limit is $2.0 M_{\odot}$. The best fit mass function significantly exceeds the canonical maximum mass of a neutron star ($3.0 M_{\odot}$), and even allowing for the shorter period alias, a black hole seems likely, especially as K_2 has probably been underestimated.

In principle, we could hope that the wings of the He II line will follow the compact object. Hence we might derive K_1 and the mass ratio. In this case, however, the He II velocities should be anti-phased with the N III ones, which is clearly not the case. Rather they are almost in phase with it, as is the overall movement of the He II line. This indicates that even the radial velocity curve of the wings is significantly contaminated by He II emission from the companion and/or the stream-impact point; the phase offset is in the direction expected for emission from the stream-impact point, as is commonly seen in other LMXBs and cataclysmic variables. At most we can then hope that the low amplitude of the observed modulation rules out a large K_1 . From the VLT data we measure a semi-amplitude of $25.7 \pm 1.4 \text{ km s}^{-1}$. If we then assume K_1 is not larger than this, then we expect a mass ratio $q \lesssim 0.08$, similar to other black hole candidates. This estimate is not secure, however, as one could imagine a situation where contamination of the radial velocity curve could cancel out a larger K_1 reducing the overall modulation to close to zero.

5. Discussion

Our estimate of the mass function is surprisingly large. It has been widely assumed that the inclination of GX 339–4 is low; hence we would expect a lower K_2 and a small mass function. The most convincing argument, by Wu et al. (2001), is based on the small peak separation of double-peaked lines. This is only weakly sensitive to our revised orbital period and is hard to discount. Interpretations of peak separations are not straightforward, however, and when the parameters are known a priori, apparent sub-Keplerian motions are often inferred (e.g. Marsh (1998)). Hence the peak separation is not a reliable diagnostic of

the system parameters. Nonetheless, the inconsistency of a small peak separation and our moderately large mass function is the most problematic feature of our interpretation.

It is puzzling, and frustrating, that sharp N III components are not present all the time, instead appearing confined to a limited phase range. This is why our radial velocity curve is incomplete, despite good orbital phase coverage. The phase range where they are seen is different at the two epochs; in our last VLT observation we see them emerge during the sequence, at around phase 0.65, whereas the NTT observations revealed them earlier than this. One possible interpretation involves variable shielding of the companion star by a warped disk. The smaller mass ratios of black hole systems compared to those containing neutron stars will reduce the angular size of the companion Roche lobe as seen by the X-ray source, so shielding by the disk will be more significant in the black hole case. If the disk is warped then each hemisphere of the companion may only be illuminated during part of the orbit, as the companion rotates around the nearly stationary warp pattern. As the warp slowly precesses, the illuminated phase range will migrate as we seem to observe. Of course, the X-ray brightness was also different at the two epochs and other changes in the irradiation geometry could also be responsible for the difference.

6. Conclusions

We have shown that optical spectroscopy of the Bowen blend and He II are consistent with an orbital period for GX 339–4 of around ~ 1.7 days. No other period is simultaneously consistent with all of the data. Furthermore, only this period gives a sensible systemic velocity for the Bowen blend lines. Bowen radial velocities reveal a large modulation that must originate from the irradiated inner face of the companion star. This implies a projected orbital velocity of $K_2 = (317 \pm 10) \text{ km s}^{-1}$ for the preferred 1.7557 day orbital period (although strictly this is a lower limit). Hence we derive a mass function of $(5.8 \pm 0.5) M_\odot$ for the compact object. For the shortest acceptable alias of the orbital period we derive a 95% confidence lower limit to the mass function of $2.0 M_\odot$. This makes GX 339–4 a new addition to the list of stellar mass black hole candidates supported by dynamical evidence. The small modulation to the wings of the He II line suggests a low mass ratio, $q \lesssim 0.08$, consistent with this interpretation, although this constraint is less secure.

RIH would like to thank Michelle Buxton, Rob Robinson, and Brad Behr for valuable discussion and criticism. RIH and PAC acknowledge support from grant F/00-180/A from the Leverhulme Trust. RIH is funded from NASA through Hubble Fellowship grant #HF-01150.01-A awarded by STScI, which is operated by the AURA, Inc., for NASA, under

contract NAS 5-26555. DS acknowledges a PPARC Postdoctoral Fellowship and a SAO Clay Fellowship. This work uses observations collected at ESO in Chile and the AAO in Australia. We would particularly like to thank the ESO Director's Office and VLT staff for a generous and efficiently executed award of Director's Discretionary Time. This work has also made use of the NASA ADS Abstract Service.

REFERENCES

- Callanan, P. J., Charles, P. A., Honey, W. B., & Thorstensen, J. R. 1992, MNRAS, 259, 395
- Cowley, A. P., Schmidtke, P. C., Hutchings, J. B., & Crampton, D. 2002, AJ, 123, 1741
- Grindlay, J. E. 1979, ApJ, 232, L33
- Horne, K. 1986, PASP, 98, 609
- McClintock, J. E., Canizares, C. R., & Tarter, C. B. 1975, ApJ, 198, 641
- Marsh, T. 1998, ASP Conf. Ser. 137: Wild Stars in the Old West, 236
- Samimi, J. et al. 1979, Nature, 278, 434
- Schneider, D. P. & Young, P. 1980, ApJ, 238, 946
- Shafter, A. W. 1983, ApJ, 267, 222
- Shahbaz, T., Fender, R., & Charles, P. A. 2001, A&A, 376, L17
- Steeghs, D. & Casares, J. 2002, ApJ, 568, 273
- Still, M. D., Quaintrell, H., Roche, P. D., & Reynolds, A. P. 1997, MNRAS, 292, 52
- Wu, K., Soria, R., Hunstead, R. W., & Johnston, H. M. 2001, MNRAS, 320, 177

Table 1: Log of spectroscopic observations of GX 339–4.

Date (2002)	Telescope	UT range	Spectra ^a	R (km s ⁻¹)
Jun 6	AAT	10:35–15:11	12	70
Jun 8	AAT	10:46–14:46	7	70
Jun 9	NTT	00:37–09:34	24(23)	60–90
Jun 9	AAT	12:01–19:40	10	70
Jun 10	NTT	01:45–05:08	7	120
Jun 10	AAT	09:31–10:35	3	70
Jun 10–11	NTT	23:52–00:41	2(2)	60–70
Jun 11	AAT	09:59–11:03	3	70
Aug 9–10	VLT	23:38–01:31	5(5)	8
Aug 10–11	VLT	23:29–01:22	5	8
Aug 11–12	VLT	23:39–01:32	5	8
Aug 13	VLT	00:11–02:04	5	8
Aug 14	VLT	02:13–04:07	5	8
Aug 14–15	VLT	23:56–01:48	5(2)	8

^aBracketed numbers refer to the number of spectra showing convincing sharp N III components.

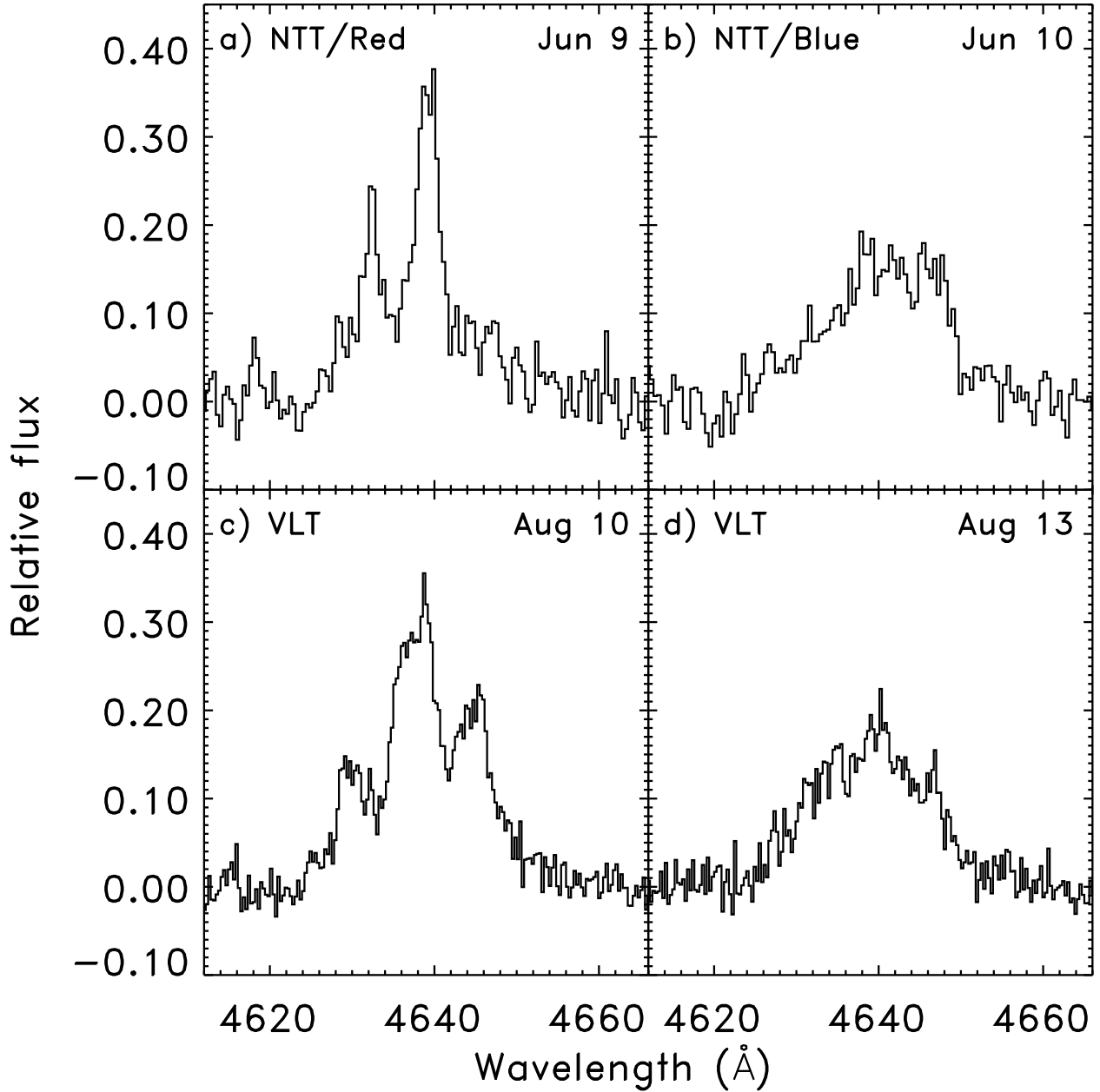


Fig. 1.— Examples of Bowen blend profiles from four different observations. The left hand two panels show profiles with sharp components; the right hand panels lack them. All spectra have been normalized and then continuum subtracted, so fluxes are relative to the continuum level.

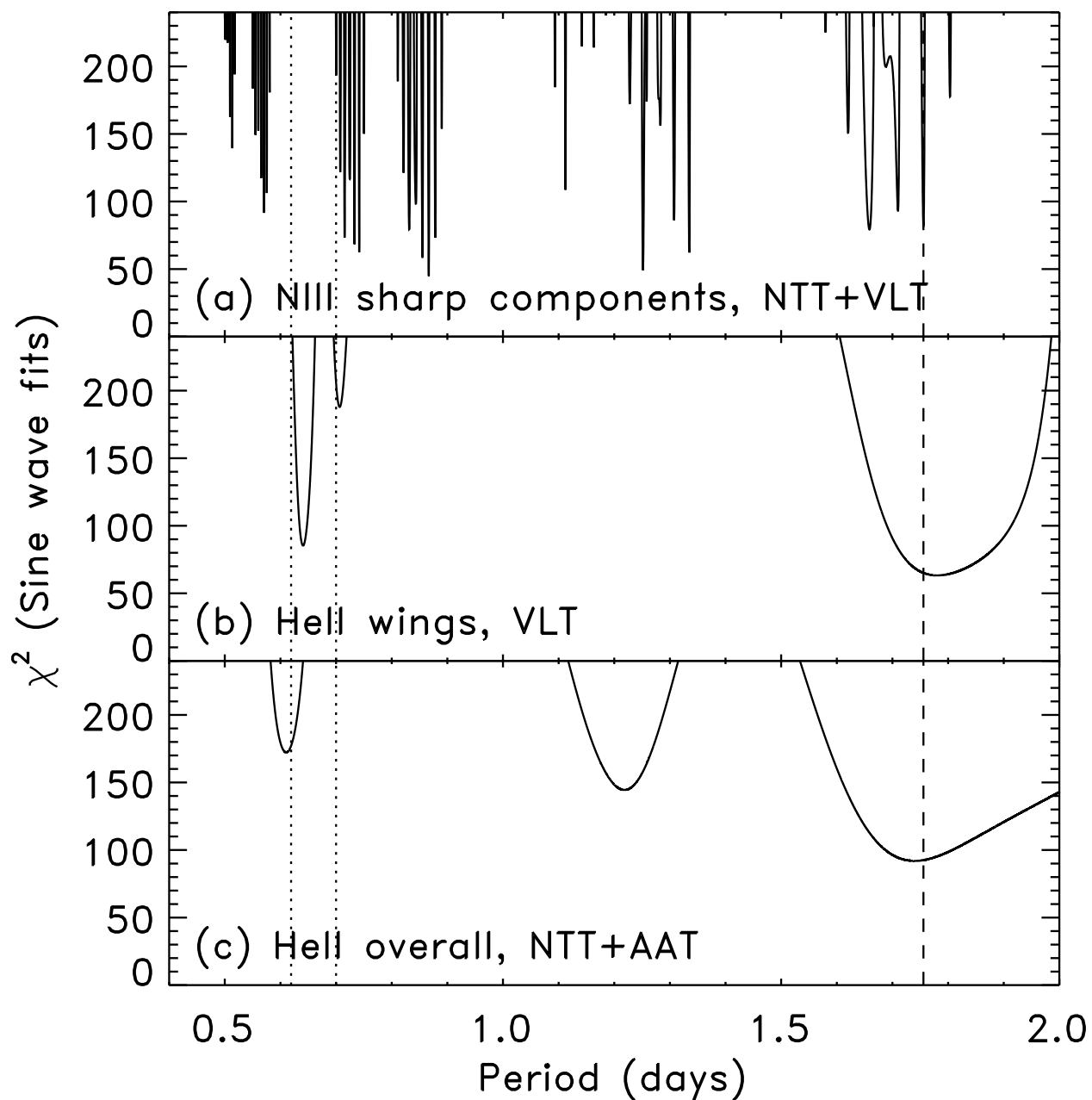


Fig. 2.— χ^2 of sinusoidal model fits as a function of orbital period. The systemic velocity, radial velocity semi-amplitude and phasing are allowed to vary to obtain the best fit of each dataset for a given orbital period. The dashed line shows our preferred 1.7557 day period; dotted lines indicate the 0.62 and 0.7 day periods of Callanan et al. (1992) and Cowley et al. (2002) respectively.

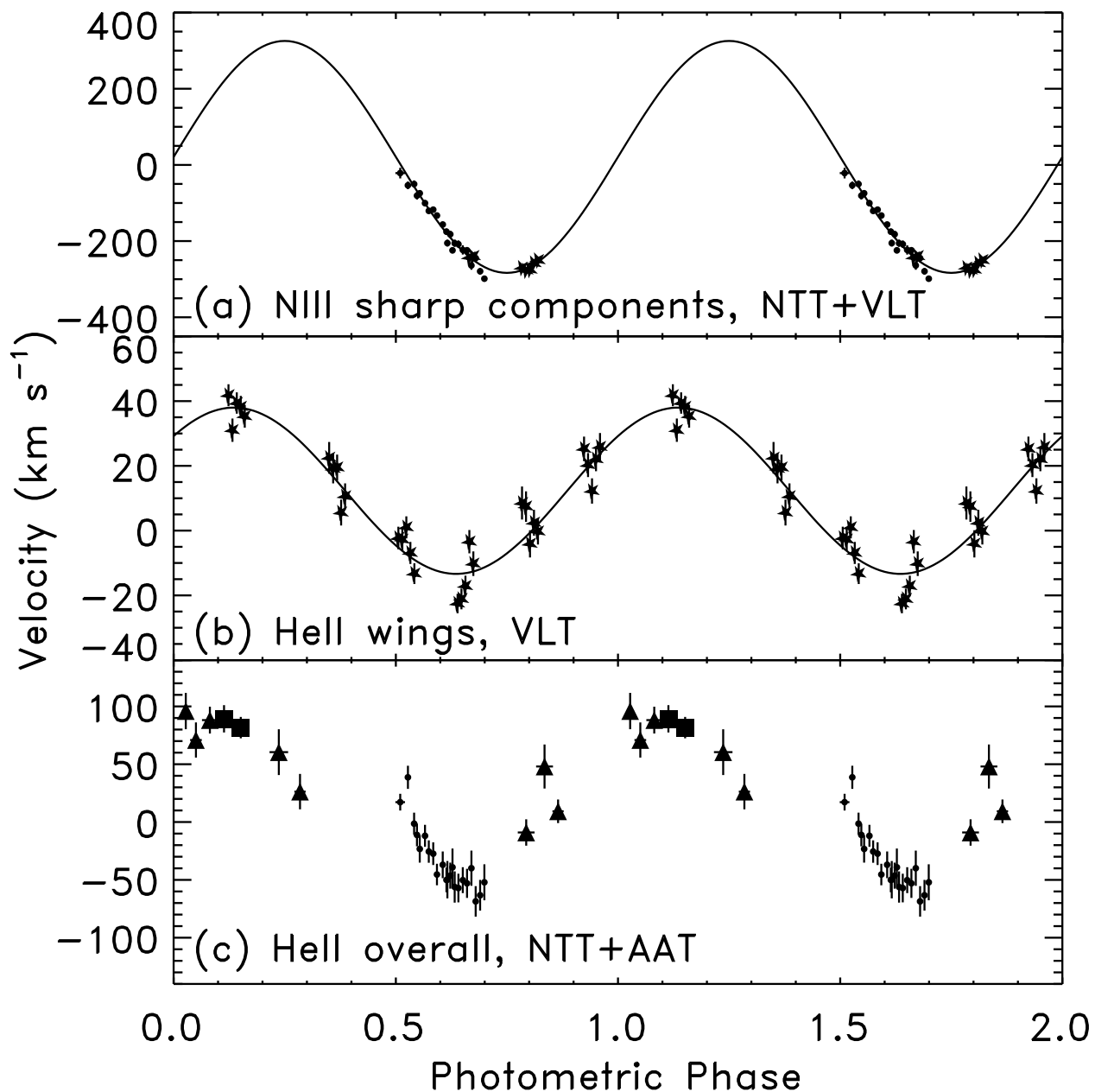


Fig. 3.— Radial velocity curves corresponding to the data used in Fig. 2, folded on our preferred 1.7557 day period. Circles denote NTT red-arm data, squares NTT blue-arm, triangles AAT, and stars VLT data. Where error-bars are not apparent, they are smaller than the points. No fit is shown for the third panel as this reflects changes in morphology more than actual motion and so the radial velocity curve has no physical significance, other than as a diagnostic of the period. Note that (b) and (c) are derived from completely independent sets of data.